Radiation dynamics of a cavitation bubble in a liquid-filled cavity surrounded by an elastic solid

Catherine Drysdale, Alexander A. Doinikov, and Philippe Marmottant
LIPhy, CNRS/Université Grenoble Alpes, F-38000 Grenoble, France
(Received 16 February 2017; published 10 May 2017)

A specific cavitation phenomenon occurs inside the stems of trees. The internal pressure in tree conduits can drop down to significant negative values, which causes the nucleation of bubbles. The bubbles exhibit high-frequency oscillations just after their nucleation. In the present study, this phenomenon is modeled by taking into account acoustic waves produced by bubble oscillations. A dispersion equation is derived, which is then used to calculate the resonance frequency and the attenuation coefficient of the bubble oscillations. Radiation damping is found to be predominant in comparison with viscous damping, except for very small bubbles. A typical number of oscillation cycles before the complete damping of the oscillation is found to be of the order of 10, as observed for cavitation bubbles in biomimetic synthetic trees.

DOI: 10.1103/PhysRevE.95.053104

I. INTRODUCTION

The motivation of the present study is to understand a peculiar acoustic phenomenon that occurs in trees. Under usual conditions, there are no spontaneous vibrations inside trees. The only motion is a quiet internal flow of aqueous sap inside a porous network of conduits. This flow is driven by evaporation taking water out of the leaves, generating very strong negative pressures (tension), on the order of several MPa [1,2], down to −18.8 MPa of absolute pressure for certain trees [3]. The downside of such negative pressures is the possibility of cavitation, i.e., the sudden generation of bubbles, which relaxes the tension in the liquid.

The time scale of the bubble growth is of the order of one microsecond [4]. As a result, the bubble reaches a temporary equilibrium radius. Although subsequently the bubble dissolves quickly enough, experimental observations show that after nucleation, it has time (of the order of several milliseconds) to perform transient oscillations and to emit acoustic waves into the surrounding medium. It should also be noted that at the initial stage, bubbles tend to grow rather than to dissolve because water can easily diffuse into the surrounding wood, which is very dry [4]. Sounds in trees were first recorded in the audible range [5] and then in the ultrasonic range [6]. It was also proposed to use acoustic recordings as a method to monitor the development of cavitation [7] after signal processing to evaluate the acoustic energy. It is important to monitor cavitation bubbles since they are catastrophic for the tree physiology; their growth results in a gaseous embolism, stopping the circulation of sap flow [8]. Cavitation is therefore believed to be a major cause for tree mortality during periods of drought [9,10]. However, in certain plants, it can be beneficial: that is the case of ferns [11], where cavitation triggers the ejection of spores. Cavitation can be initiated experimentally. For instance, it was proved that cavitation indeed occurred in joints ("cracking" joints) [12], which is harmless according to a statistical study [13].

The pitch (frequency) of the acoustic emission is linked to the vibration of a bubble after nucleation. This vibration frequency was predicted using a quasistatic model [14,15], assuming that the sound wavelength is very large and thus neglecting any acoustic propagation effects.

The goal of the present study is to develop a theoretical model for acoustic emissions produced by cavitation bubbles inside trees. This model is necessary to predict the frequency and attenuation of sound, which would be helpful for understanding the acoustic signals emitted.

II. MODEL

In the problem under study, the bubble oscillation is caused by a drop of the ambient pressure within a space whose dimensions are much greater than the bubble size. In this case, physically, the dominant mode of the bubble motion is the breathing mode. Therefore, we solve the problem in the approximation of spherical symmetry. Following this approximation, we consider a spherical bubble that is located at the center of a spherical cavity, as shown in Fig. 1, and undergoes monopole oscillations. We assume that the cavity is filled with a compressible viscous liquid, the medium surrounding the cavity is an elastic solid, and the medium inside the bubble is vacuum. The bubble nucleation in water at a negative pressure of several MPa is a very fast process. Its duration can be less than one microsecond [4]. Therefore, initially the bubble has a very low gas content, with remaining ballistic water molecules. It is only afterward that the bubble is filled with water vapor evaporating from the bubble surface and then with air diffusing from water. This allows one to treat the bubble interior as vacuum. The liquid mass is assumed to be constant as the diffusion of water into the surrounding wood is a slow process in comparison with the bubble nucleation.

A. Liquid equations

In the linear approximation, the motion of the liquid filling the cavity is described by the following equations [16]:

$$\rho_0 \frac{\partial \boldsymbol{v}}{\partial t} = -\nabla p + \eta \Delta \boldsymbol{v} + \left(\zeta + \frac{1}{3}\eta\right)\nabla(\nabla \cdot \boldsymbol{v}), \tag{1}$$

$$\frac{\partial \rho}{\partial t} + \rho_0 \nabla \cdot \boldsymbol{v} = \boldsymbol{0}, \tag{2}$$

$$p = c^2 \rho. \tag{3}$$

Here, $\boldsymbol{v}$ is the liquid velocity, p is the perturbed liquid pressure, η is the shear viscosity, ζ is the bulk viscosity, ρ is the perturbed

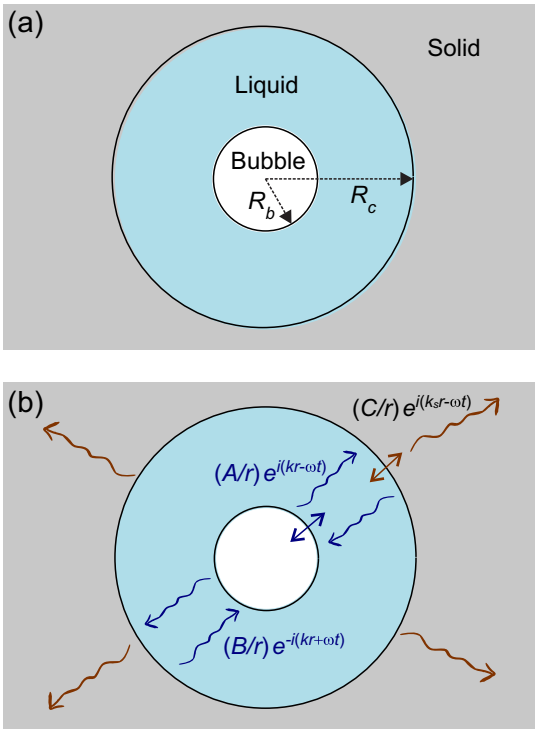

FIG. 1. (a) The system under study: the nucleation of a cavitation bubble in a liquid-filled cavity that leads to the relaxation of tension in the liquid. (b) Acoustic waves induced by the bubble pulsation after nucleation.

liquid density, ρ_0 is the liquid density at rest, and c is the speed of sound. Equations (1)–(3) are the compressible Navier-Stokes equation, the continuity equation, and the equation of state, respectively.

In view of spherical symmetry, the liquid motion is irrotational and hence one can set $\boldsymbol{v} = \nabla\varphi$. Assuming that the time dependence is $\exp(-i\omega t)$, one can transform Eqs. (1)–(3) to the Helmholtz equation,

$$\Delta\varphi + k^2\varphi = 0, \tag{4}$$

where k is defined as

$$k = \frac{\omega}{c}\left[1 - \frac{i\omega}{\rho_0 c^2}\left(\zeta + \frac{4}{3}\eta\right)\right]^{-\frac{1}{2}}. \tag{5}$$

A spherically symmetrical solution to Eq. (4) is written as

$$\varphi = \frac{A}{r}e^{i(kr-\omega t)} + \frac{B}{r}e^{-i(kr+\omega t)}, \tag{6}$$

where A and B are constants to be determined by boundary conditions. Equation (6) describes the outgoing wave and the wave reflected by the liquid-solid boundary. They are depicted in Fig. 1(b). It follows from Eq. (6) that the liquid velocity has only the radial component, which is calculated by

$$v = \frac{\partial\varphi}{\partial r} = A\left(\frac{ik}{r} - \frac{1}{r^2}\right)e^{i(kr-\omega t)} - B\left(\frac{ik}{r} + \frac{1}{r^2}\right)e^{-i(kr+\omega t)}. \tag{7}$$

To satisfy the boundary conditions, an expression for the normal stress in the liquid is also required. It is given by

$$\sigma_{rr} = -p + 2\eta\frac{\partial v}{\partial r} + \left(\zeta - \frac{2}{3}\eta\right)\nabla\cdot\boldsymbol{v}. \tag{8}$$

It follows from Eqs. (2)–(4) that

$$p = \frac{i\rho_0 c^2 k^2}{\omega}\varphi. \tag{9}$$

Substituting Eqs. (7) and (9) into Eq. (8) and using Eq. (5), one obtains

$$\sigma_{rr} = -A\left(\frac{i\rho_0\omega}{r} + \frac{4i\eta k}{r^2} - \frac{4\eta}{r^3}\right)e^{i(kr-\omega t)} - B\left(\frac{i\rho_0\omega}{r} - \frac{4i\eta k}{r^2} - \frac{4\eta}{r^3}\right)e^{-i(kr+\omega t)}. \tag{10}$$

B. Solid equations

The motion of the solid is assumed to be Hookean and governed by the Navier equation [17],

$$\rho_s\frac{\partial^2\boldsymbol{u}}{\partial t^2} = \mu\Delta\boldsymbol{u} + (\lambda+\mu)\nabla(\nabla\cdot\boldsymbol{u}), \tag{11}$$

where $\boldsymbol{u}$ is the displacement vector, ρ_s is the density of the solid, and λ and μ are the Lamé coefficients. The spherical symmetry allows one to set $\boldsymbol{u} = \nabla\varphi_s$. As a consequence, Eq. (11) is transformed to

$$\Delta\varphi_s + k_s^2\varphi_s = 0, \tag{12}$$

where

$$k_s = \frac{\omega}{c_s}, \quad c_s = \sqrt{\frac{\lambda+2\mu}{\rho_s}}, \tag{13}$$

and c_s is known as the longitudinal wave speed. A solution to Eq. (12) is written as

$$\varphi_s = \frac{C}{r}e^{i(k_s r-\omega t)}, \tag{14}$$

where C is a constant to be determined. The outgoing wave given by Eq. (14) is depicted in Fig. 1(b). The radial component of $\boldsymbol{u}$ is calculated by

$$u = C\left(\frac{ik_s}{r} - \frac{1}{r^2}\right)e^{i(k_s r-\omega t)}. \tag{15}$$

Lastly, the normal stress in the solid is defined by

$$\tau_{rr} = \lambda\nabla\cdot\boldsymbol{u} + 2\mu\frac{\partial u}{\partial r}. \tag{16}$$

Substitution of Eq. (15) into Eq. (16) yields

$$\tau_{rr} = -C\left[\frac{k_s^2}{r}(\lambda+2\mu) + 4\mu\left(\frac{ik_s}{r^2} - \frac{1}{r^3}\right)\right]e^{i(k_s r-\omega t)}. \tag{17}$$

C. Boundary conditions

The boundary conditions involve zero normal stress at the bubble surface, and the continuity of velocity and normal stress at the liquid-solid interface:

$$\sigma_{rr} = 0 \quad \text{at } r = R_b, \tag{18}$$

$$v = \frac{\partial u}{\partial t} \quad \text{at } r = R_c, \tag{19}$$

$$\sigma_{rr} = \tau_{rr} - P_a e^{-i\omega t} \quad \text{at } r = R_c, \tag{20}$$

where R_b is the equilibrium bubble radius, R_c is the equilibrium radius of the cavity, and P_a is the amplitude of the driving acoustic pressure in the case of forced oscillations.

As one can see, we have not included the surface tension pressure in Eqs. (18) and (20). The reason is that there is no well-reasoned, generally recognized opinion among researchers about the effect of surface tension at liquid-solid and liquid-vacuum (strongly rarefied gas) interfaces in cases similar to that considered here [18,19]. There are no reliable methods for measuring the value of interfacial tension at liquid-solid interfaces, and therefore there are no valid data for this quantity, especially in such complex cases as the contact of wood and water. The question as to what is the value of surface tension between a liquid and vacuum is disputed as well. One opinion is that this value should be close to that between the liquid and air under normal conditions. However, another opinion is that this value may be much lower as the liquid intensively evaporates for a great difference in pressures. Therefore, the surface tension pressure is often neglected in equations similar to ours [20–22], assuming that its role is secondary and cannot change the essential physics of the process under study.

Substitution of Eqs. (7), (10), (15), and (17) into Eqs. (18)–(20) gives a system of algebraic equations in the unknowns A, B, and C,

$$\begin{pmatrix} a_{11} & a_{12} & a_{13} \\ a_{21} & a_{22} & a_{23} \\ a_{31} & a_{32} & a_{33} \end{pmatrix} \begin{pmatrix} A \\ B \\ C \end{pmatrix} = \begin{pmatrix} 0 \\ 0 \\ P_a \end{pmatrix}. \tag{21}$$

The matrix elements a_{nm} are calculated by

$$\begin{aligned}
&a_{11} = \left[1 + 2\xi_b^2(i + kR_b)\right]e^{ikR_b}, \qquad a_{12} = \left[1 + 2\xi_b^2(i - kR_b)\right]e^{-ikR_b}, \qquad a_{13} = 0, \\
&a_{21} = (ikR_c - 1)e^{ikR_c}, \qquad a_{22} = -(ikR_c + 1)e^{-ikR_c}, \qquad a_{23} = i\omega(ik_sR_c - 1)e^{ik_sR_c}, \\
&a_{31} = i\rho_0\omega R_c^{-1}\left[1 + 2\xi_c^2(i + kR_c)\right]e^{ikR_c}, \qquad a_{32} = i\rho_0\omega R_c^{-1}\left[1 + 2\xi_c^2(i - kR_c)\right]e^{-ikR_c}, \\
&a_{33} = -R_c^{-3}[(\lambda + 2\mu)(k_sR_c)^2 + 4\mu(ik_sR_c - 1)]e^{ik_sR_c},
\end{aligned} \tag{22}$$

where

$$\xi_b = \frac{\delta}{R_b}, \qquad \xi_c = \frac{\delta}{R_c}, \qquad \delta = \sqrt{\frac{2\eta}{\rho_0\omega}}, \tag{23}$$

and δ is known as the viscous penetration depth. In many cases of interest, $\xi_{b,c} \ll 1$; see examples in Sec. III.

D. Free oscillations

In the case of free oscillations, such as those right after the bubble nucleation, $P_a = 0$. In this case, the system of Eqs. (21) has a nontrivial solution only if its determinant is equal to zero. This condition gives an equation for calculating ω,

$$\begin{aligned}
&\left\{1 - kR_c\cot(kR_c - kR_b)\left[1 + 2i\xi_b^2\left(1 - \frac{R_b}{R_c}\right)\right]\right. \\
&\quad \left. + 2i\xi_b^2(1 + k^2R_bR_c)\right\}\left[\frac{4\mu}{\rho_s c_s^2}(1 - ik_sR_c) - (k_sR_c)^2\right] \\
&\quad + \frac{\rho_0}{\rho_s}(k_sR_c)^2(1 - ik_sR_c)\left[1 + 2i\xi_b^2\left(1 + \frac{R_b^2}{R_c^2}\right)\right. \\
&\quad - 4\xi_b^2\xi_c^2(1 + k^2R_bR_c) \\
&\quad \left. + 2ikR_c\xi_b^2\left(1 - \frac{R_b}{R_c}\right)\left(\frac{R_b}{R_c} - 2i\xi_c^2\right)\cot(kR_c - kR_b)\right] \\
&= 0.
\end{aligned} \tag{24}$$

Recall that k and k_s are functions of ω given by Eqs. (5) and (13). In the general case, ω is a complex number whose real part is the resonance frequency of the system and the imaginary part is the attenuation coefficient. Approximate analytical solutions to the dispersion equation (24) will be derived in Sec. II F and exact numerical solutions will be considered in Sec. III.

It is pertinent to note that in the case of a rigid solid ($\rho_s \to \infty$) and negligible liquid viscosity ($\eta = 0$), we recover a simpler dispersion equation derived in [15]: $1 - kR_c\cot(kR_c - kR_b) = 0$.

E. Forced oscillations

For the sake of completeness, we also consider the case of forced oscillations, where $P_a \neq 0$ and ω is a known quantity. In this case, the system of Eqs. (21) allows one to calculate the constants A, B, and C,

$$A = \frac{i\omega P_a}{D}(ik_sR_c - 1)\left[1 + 2\xi_b^2(i - kR_b)\right]e^{i(k_sR_c - kR_b)}, \tag{25}$$

$$B = \frac{i\omega P_a}{D}(1 - ik_sR_c)\left[1 + 2\xi_b^2(i + kR_b)\right]e^{i(k_sR_c + kR_b)}, \tag{26}$$

$$\begin{aligned}
C = \frac{P_a}{D}\{&(1 - ikR_c)\left[1 + 2\xi_b^2(i - kR_b)\right]e^{ik(R_c - R_b)} \\
&- (1 + ikR_c)\left[1 + 2\xi_b^2(i + kR_b)\right]e^{-ik(R_c - R_b)}\},
\end{aligned} \tag{27}$$

where D is given by

$$\begin{aligned} D = {} & \frac{\rho_s c_s^2}{R_c^3} e^{ik_s R_c}\left[(k_s R_c)^2 + \frac{4\mu}{\rho_s c_s^2}(ik_s R_c - 1)\right] \\ & \times \left\{(ikR_c - 1)\left[1 + 2\xi_b^2(i - kR_b)\right]e^{ik(R_c - R_b)}\right. \\ & \left. + (ikR_c + 1)\left[1 + 2\xi_b^2(i + kR_b)\right]e^{-ik(R_c - R_b)}\right\} \\ & - \frac{\rho_0\omega^2}{R_c}(ik_s R_c - 1)e^{ik_s R_c} \\ & \times \left\{\left[1 + 2\xi_b^2(i - kR_b)\right]\left[1 + 2\xi_c^2(i + kR_c)\right]e^{ik(R_c - R_b)}\right. \\ & \left. - \left[1 + 2\xi_b^2(i + kR_b)\right]\left[1 + 2\xi_c^2(i - kR_c)\right]e^{-ik(R_c - R_b)}\right\}. \end{aligned} \tag{28}$$

F. Approximate solutions of the dispersion equation

In this subsection, we derive approximate analytical solutions to the dispersion equation (24), assuming that $kR_{b,c}$, $k_s R_c$, $\xi_{b,c} \ll 1$.

1. Second-order approximation

Let us first expand Eq. (24) up to second order in $kR_{b,c}$ and $k_s R_c$. Correct to leading viscous terms, the result is a quadratic equation in ω,

$$\omega^2 + 2i\alpha_0\omega - \omega_0^2 = 0, \tag{29}$$

where

$$\omega_0 = \frac{2}{R_c}\sqrt{\frac{\mu R_b}{\rho_0\beta(R_c - R_b)}}, \tag{30}$$

$$\beta = 1 + \frac{4\mu}{3\rho_0 c^2}\left(1 - \frac{R_b}{R_c}\right) + \frac{\rho_s R_b}{\rho_0(R_c - R_b)}, \tag{31}$$

$$\begin{aligned} \alpha_0 = {} & \frac{2}{\rho_0\beta}\left[\frac{\mu R_b}{c_s R_c(R_c - R_b)} + \frac{\eta}{R_b^2}\left(1 + \frac{4\mu}{3\rho_0 c^2}\right)\right. \\ & \left. \times \left(1 + \frac{R_b}{R_c} + \frac{R_b^2}{R_c^2}\right)\right]. \end{aligned} \tag{32}$$

A solution to Eq. (29) is given by

$$\omega = -i\alpha_0 + \omega_0\sqrt{1 - \frac{\alpha_0^2}{\omega_0^2}}. \tag{33}$$

The resonance frequency is defined as $f_r = \mathrm{Re}[\omega]/2\pi$ and the attenuation coefficient is equal to α_0.

An interesting conclusion can be drawn from Eq. (30). For the case of a bubble in an unbounded liquid, the presence of gas inside the bubble is required to obtain free oscillations, inasmuch as the gas compressibility provides a restoring force [23]. Equation (30) shows that for the case of a bubble in a solid, the gas filling is not essential because the restoring force is provided by the solid elasticity.

Equation (32) allows one to estimate the relative contributions of the radiation and viscous losses. It shows that for $R_b/R_c \ll 1$, the viscous attenuation becomes dominant when

$$R_b < \sqrt[3]{\frac{\eta c_s R_c^2}{\mu}\left(1 + \frac{4\mu}{3\rho_0 c^2}\right)}. \tag{34}$$

For experimental parameters used in [14,15], Eq. (34) gives $R_b < 2.8\ \mu$m.

2. Third-order approximation

Comparison with exact numerical solutions given by Eq. (24) (see Sec. III) shows that Eq. (33) provides a satisfactory approximation for the resonance frequency. However, as far as the attenuation coefficient is concerned, Eq. (32) fails at intermediate values of the ratio R_b/R_c, probably because $kR_{b,c}$ or $k_s R_c$ are not small enough. To improve the approximate equation for the attenuation coefficient, it is necessary to keep compressible terms in Eq. (24) up to third order in $kR_{b,c}$ and $k_s R_c$. Doing so, with an accuracy to leading viscous terms, one obtains a cubic equation in ω,

$$a_1\omega^3 + a_2\omega^2 + a_3\omega + a_4 = 0, \tag{35}$$

where

$$a_1 = -\frac{iR_c}{c_s}\left[1 + \frac{4\mu}{3\rho_0 c^2}\left(1 - \frac{R_b}{R_c}\right)\right], \tag{36}$$

$$\begin{aligned} a_2 = {} & 1 + \frac{4\mu}{3\rho_0 c^2}\left(1 - \frac{R_b}{R_c}\right) + \frac{\rho_s R_b}{\rho_0(R_c - R_b)} \\ & + \frac{4\eta R_c}{\rho_0 c_s R_b^2}\left(1 + \frac{4\mu}{3\rho_0 c^2}\right)\left(1 + \frac{R_b}{R_c} + \frac{R_b^2}{R_c^2}\right), \end{aligned} \tag{37}$$

$$\begin{aligned} a_3 = {} & \frac{4i}{\rho_0}\left[\frac{\mu R_b}{c_s R_c(R_c - R_b)} + \frac{\eta}{R_b^2}\left(1 + \frac{4\mu}{3\rho_0 c^2}\right)\right. \\ & \left. \times \left(1 + \frac{R_b}{R_c} + \frac{R_b^2}{R_c^2}\right)\right], \end{aligned} \tag{38}$$

$$a_4 = -\frac{4\mu R_b}{\rho_0 R_c^2(R_c - R_b)}. \tag{39}$$

Equation (35) has three roots. However, in our case only one of them has a positive real part, which is the necessary condition to get a physical value for the resonance frequency. This root is calculated by Cardan's formulas as follows:

$$p = \frac{a_3}{a_1} - \frac{a_2^2}{3a_1^2}, \tag{40}$$

$$q = \frac{2a_2^3}{27a_1^3} - \frac{a_2 a_3}{3a_1^2} + \frac{a_4}{a_1}, \tag{41}$$

$$s = \sqrt[3]{-\frac{q}{2} + \sqrt{\left(\frac{p}{3}\right)^3 + \left(\frac{q}{2}\right)^2}}, \tag{42}$$

$$\omega = s - \frac{p}{3s} - \frac{a_2}{3a_1}. \tag{43}$$

G. Limiting cases

The second-order approximation provides relatively simple equations for the resonance frequency, which, as will be shown in Sec. III, are in satisfactory agreement with exact numerical solutions given by Eq. (24). Therefore, we use these equations here to consider limiting cases of interest.

For an inviscid liquid ($\eta = 0$), the second-order solution given by Eq. (33) reduces to

$$\omega = -\frac{i\omega_0^2 R_c}{2c_s} + \omega_0\sqrt{1-\left(\frac{\omega_0 R_c}{2c_s}\right)^2}. \tag{44}$$

If the bubble radius is small compared to the cavity radius, $R_b/R_c \ll 1$, Eq. (30) for ω_0 is simplified to

$$\omega_0 = \frac{1}{R_c}\sqrt{\frac{3R_b}{\rho_0 R_c}\,\frac{\rho_0 c^2 \times 4\rho_s c_t^2/3}{\rho_0 c^2 + 4\rho_s c_t^2/3}}, \tag{45}$$

where $c_t = \sqrt{\mu/\rho_s}$ denotes the speed of transverse waves in the solid. Note that ω_0 is the so-called undamped natural frequency, i.e., the resonance frequency in the case of negligible damping. Equation (45) reproduces the quasistatic prediction obtained in [15], which was derived for $k_s R_c \to 0$.

If the bubble radius tends to the cavity radius, $R_b \to R_c$, Eq. (44) gives the following equations for the natural frequency and the attenuation coefficient:

$$\omega_0 = \frac{2c_t}{R_c}, \quad \alpha_0 = \frac{c_t}{c_s}, \tag{46}$$

which reproduce the results obtained in [17] for the vibration of a void filled with vacuum in a solid.

In the case of a rigid solid ($\mu \to \infty$), Eq. (44) reduces to

$$\omega = \frac{c}{R_c - R_b}\sqrt{\frac{3R_b}{R_c}}. \tag{47}$$

For $R_b/R_c \ll 1$, this equation becomes even simpler,

$$\omega = \frac{c}{R_c}\sqrt{\frac{3R_b}{R_c}}. \tag{48}$$

III. NUMERICAL SIMULATIONS

The results presented in Fig. 2 were obtained at the following values of the physical parameters: $\rho_0 = 1000$ kg/m^3, $c = 1500$ m/s, $\eta = 0.001$ Pa s, $\rho_s = 1233$ kg/m^3, $c_s = 2111$ m/s, $\mu = 0.74$ GPa, and $R_c = 100$ μm. These values were chosen to reproduce cavitation experiments on transparent biomimetic wood [14,15].

Figure 2 shows the resonance frequency, $f_r = \mathrm{Re}[\omega]/2\pi$, the attenuation coefficient, $\alpha = -\mathrm{Im}[\omega]$, and the quality factor, $Q = \mathrm{Re}[\omega]/2\alpha$, as functions of the ratio R_b/R_c. The solid lines depict the numerical results calculated by Eq. (24), the long-dashed lines are provided by Eq. (33) (second-order approximation), and the short-dashed lines are given by Eq. (43) (third-order approximation). The dash-dotted lines show results given by Eq. (24) in the case of an inviscid liquid ($\eta = 0$). As one can see in Fig. 2(a), the resonance frequency increases with increasing the ratio R_b/R_c until reaching the value given by Eq. (46). The calculation also reveals that ω becomes purely imaginary when the bubble radius is smaller than 1.16 μm, which results in the extinction of the resonance frequency. This happens because the viscous losses make the system overdamped. According to Fig. 2(a), the resonance frequency of a bubble with $R_b = 20$ μm is about 1 MHz. For this case, one obtains $\xi_b \approx 0.028$ and $\xi_c \approx 0.0056$. Thus these quantities are really small compared to unity, as was said in Sec. II C.

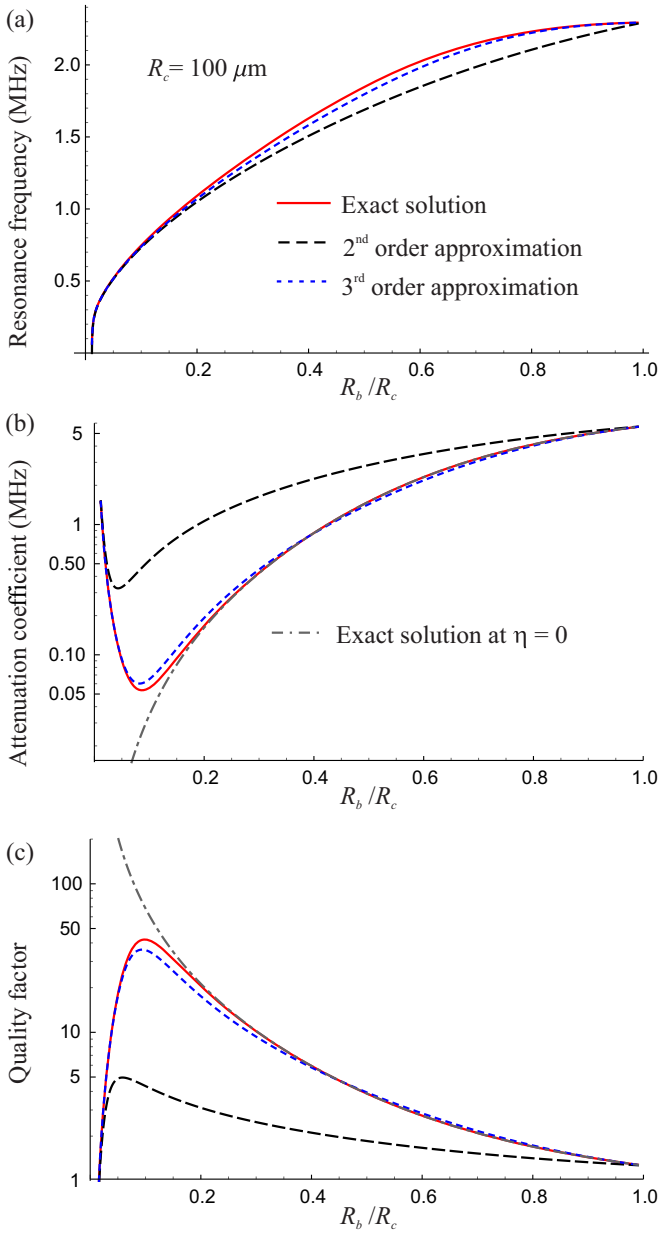

FIG. 2. Comparison of exact numerical solutions calculated by Eq. (24) (solid) with approximate analytical solutions calculated by Eq. (33) (long dashed) and Eq. (43) (short dashed). The dash-dotted lines show numerical solutions at $\eta = 0$.

The behavior of the attenuation coefficient is shown in Fig. 2(b). It is seen that the attenuation coefficient passes through a minimum. As a result, the quality factor has a maximum; see Fig. 2(c). The dash-dotted curves in Figs. 2(b) and 2(c) reveal that the viscous damping is very important at small values of R_b. Its neglect leads to a great underestimation of attenuation and hence overestimating the quality factor when R_b/R_c is smaller than 0.2. As regards the approximate solutions, Fig. 2 shows that the second-order approximation is quite correct for the resonance frequency but fails for the attenuation coefficient. However, the third-order approximation does a good job for the full range of bubble radii.

Figures 3 and 4 illustrate the reaction of the system to variation in the parameters of the solid. Figure 3 shows the effect of

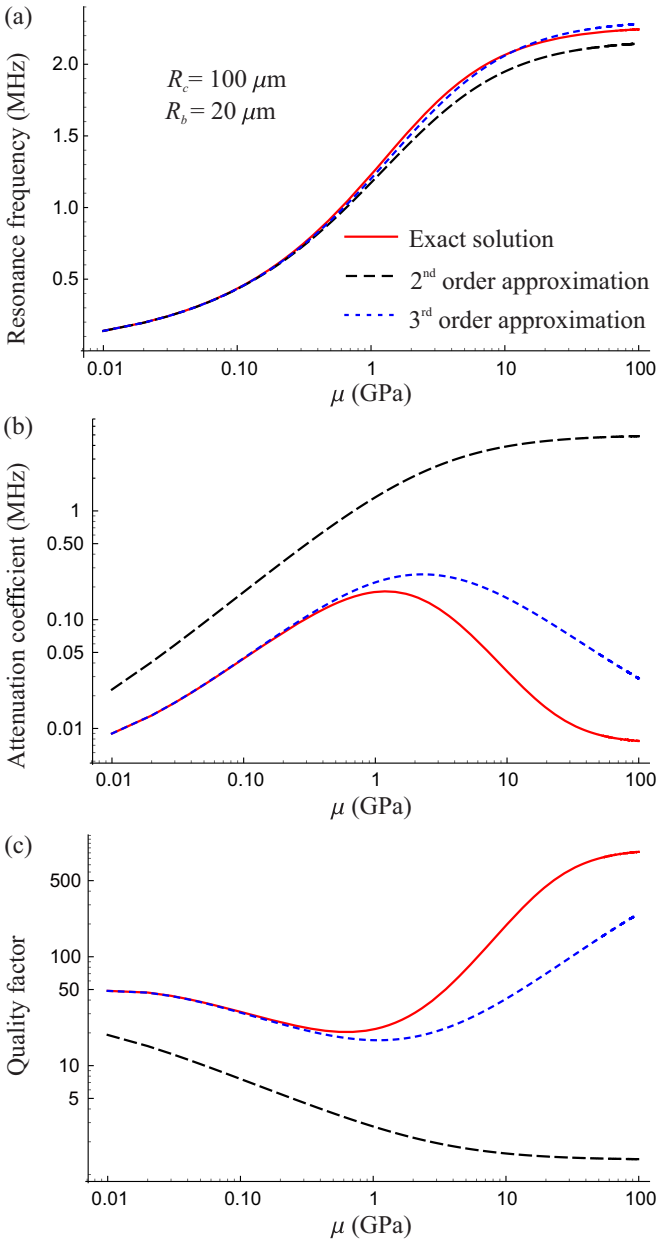

FIG. 3. Dependence on the shear modulus μ. The resonance frequency increases monotonically with μ while the attenuation coefficient passes through a maximum.

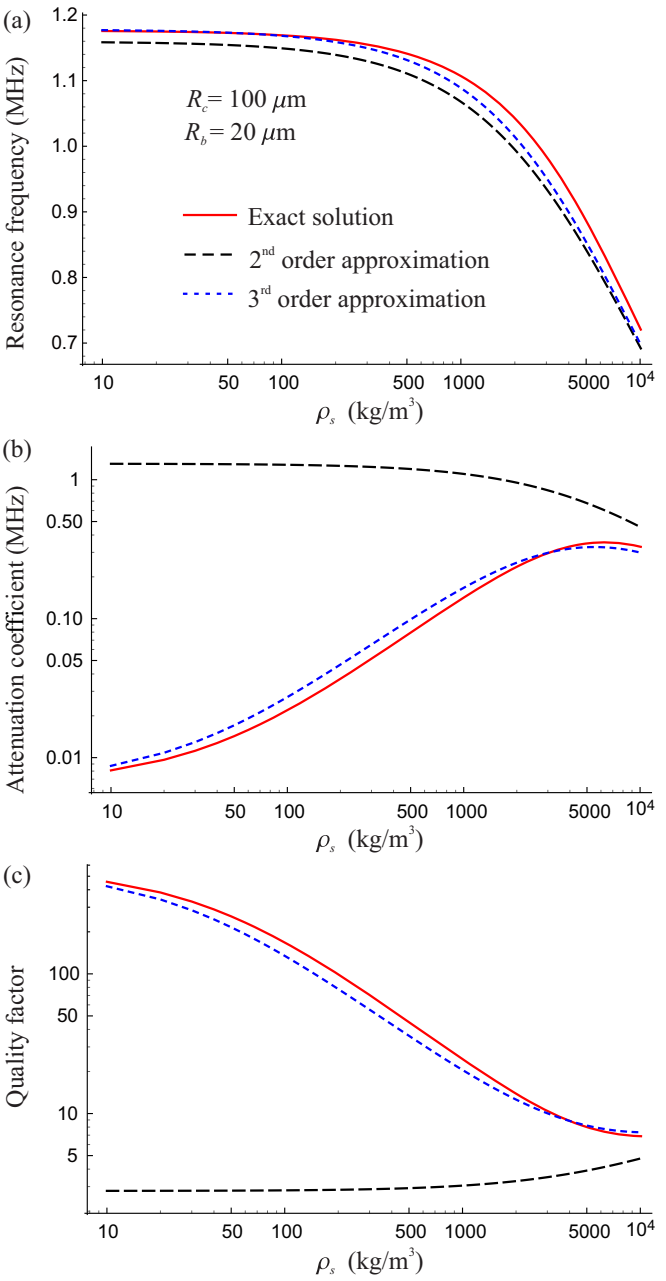

FIG. 4. Dependence on the solid density ρ_s. The resonance frequency decreases with ρ_s while the attenuation coefficient increases.

the shear modulus μ. The plots were calculated at $R_b = 20\,\mu$m, varying μ from 0.01 to 100 GPa, the other parameters being as in Fig. 2. It is seen that the resonance frequency increases monotonically with μ, while the attenuation coefficient passes through a maximum. The existence of the maximum suggests that at a certain value of μ, more energy is carried away by acoustic waves to infinity. The maximum is observed at $\mu \approx 1.5$ GPa. This value corresponds to shear moduli of real wood, which lie in the range from 1 to a few GPa.

Figure 4 shows the effect of the solid density ρ_s. The results were obtained at $R_b = 20\ \mu$m, varying ρ_s from 10 to 10 000 kg/m^3, the other parameters being as in Fig. 2. It is seen that the resonance frequency decreases with ρ_s, while the attenuation coefficient increases.

IV. CONCLUSION AND PERSPECTIVES

A theoretical model has been developed that describes acoustic emissions produced by bubbles, created through cavitation, in tree conduits. The model was used to calculate the attenuation coefficient of free bubble oscillations. It was shown that radiation damping is the main cause of attenuation for bubbles with a radius in the range of tens of micrometers, whereas viscous damping is important only for very small bubbles.

It was found that the attenuation coefficient is rather low. A typical number of oscillation cycles, which follows from the quality factor, is on the order of 10 for $R_b/R_c = 0.3$. This value is in agreement with experimental measurements [14]. As a consequence, cavitation bubbles in confinements "ring"

for a significant amount of time, which makes it possible to determine the frequency with sufficient accuracy.

Approximate analytical solutions to the dispersion equation were obtained. It was shown that the second-order approximation predicts precisely enough the resonance frequency but cannot provide correct values for the attenuation coefficient, and hence the quality factor, within the entire range of bubble radii. This problem is solved by the third-order approximation.

As a perspective, it would be helpful to include the gas content of bubbles in the theoretical model. This would allow the modeling of resonance at later stages of the bubble evolution, when bubbles are filled with gas dissolved in the surrounding liquid.

ACKNOWLEDGMENTS

This research has received funding from the European Research Council under the European Union's Seventh Framework Programme (FP7/2007-2013)/ERC Grant Agreement No. 614655 "Bubbleboost."

[1] A. D. Stroock, V. V. Pagay, M. A. Zwieniecki, and N. M. Holbrook, Annu. Rev. Fluid Mech. **46**, 615 (2014).
[2] K. H. Jensen, K. Berg-Sørensen, H. Bruus, N. M. Holbrook, J. Liesche, A. Schulz, M. A. Zwieniecki, and T. Bohr, Rev. Mod. Phys. **88**, 035007 (2016).
[3] M. Larter, T. J. Brodribb, S. Pfautsch, R. Burlett, and H. Cochard, Plant Physiol. **168**, 804 (2015).
[4] O. Vincent, P. Marmottant, P. A. Quinto-Su, and C.-D. Ohl, Phys. Rev. Lett. **108**, 184502 (2012).
[5] J. A. Milburn and R. P. C. Johnson, Planta **69**, 43 (1966).
[6] M. T. Tyree and M. A. Dixon, Plant Physiol. **72**, 1094 (1983).
[7] S. Mayr and S. Rosner, Tree Physiol. **31**, 59 (2011).
[8] M. T. Tyree and J. S. Sperry, Annu. Rev. Plant Phys. Mol. Bio. **40**, 19 (1989).
[9] T. J. Brodribb and H. Cochard, Plant Physiol. **149**, 575 (2009).
[10] B. Choat *et al.*, Nature **491**, 752 (2012).
[11] X. Noblin, N. O. Rojas, J. Westbrook, C. Lorens, M. Argentina, and J. Dumais, Science **335**, 1322 (2012).
[12] G. N. Kawchuk, J. Fryer, J. L. Jaremko, H. Zeng, L. Rowe, and R. Thompson, PLoS ONE **10**, e0119470 (2015).
[13] K. Deweber, M. Olszewski, and R. Ortolano, J. Am. Board Fam. Med. **24**, 169 (2011).
[14] O. Vincent, P. Marmottant, S. R. Gonzalez-Avila, K. Ando, and C.-D. Ohl, Soft Matter **10**, 1455 (2014).
[15] O. Vincent and P. Marmottant, J. Fluid Mech. (to be published).
[16] L. D. Landau and E. M. Lifshitz, *Fluid Mechanics* (Pergamon, Oxford, 1987).
[17] L. D. Landau and E. M. Lifshitz, *Theory of Elasticity* (Pergamon, Oxford, 1970).
[18] *Surface and Interfacial Tension: Measurement, Theory, and Applications*, edited by S. Hartland (Marcel Dekker, New York, 2004).
[19] B. Lautrup, *Physics of Continuous Matter: Exotic and Everyday Phenomena in the Macroscopic World* (CRC, Boca Raton, FL, 2011).
[20] Lord Rayleigh, Philos. Mag. **34**, 94 (1917).
[21] L. Trilling, J. Appl. Phys. **23**, 14 (1952).
[22] R. Hickling and M. S. Plesset, Phys. Fluids **7**, 7 (1964).
[23] M. Minnaert, Philos. Mag. **16**, 235 (1933).